The Ca-activated Cl Channel and its Control in Rat Olfactory Receptor Neurons

Johannes Reisert,[1,2] Paul J. Bauer,[1] King-Wai Yau,[2] and Stephan Frings[3]

[1]Institut für Biologische Informationsverarbeitung, Forschungszentrum Jülich, 52425 Jülich, Germany
[2]Howard Hughes Medical Institute and Department of Neuroscience, Johns Hopkins University School of Medicine, Baltimore, MD 21205
[3]Abteilung Molekulare Physiologie, Universität Heidelberg, Im Neuenheimer Feld 230, 69120 Heidelberg, Germany

ABSTRACT Odorants activate sensory transduction in olfactory receptor neurons (ORNs) via a cAMP-signaling cascade, which results in the opening of nonselective, cyclic nucleotide–gated (CNG) channels. The consequent Ca^{2+} influx through CNG channels activates Cl channels, which serve to amplify the transduction signal. We investigate here some general properties of this Ca-activated Cl channel in rat, as well as its functional interplay with the CNG channel, by using inside-out membrane patches excised from ORN dendritic knobs/cilia. At physiological concentrations of external divalent cations, the maximally activated Cl current was ~30 times as large as the CNG current. The Cl channels on an excised patch could be activated by Ca^{2+} flux through the CNG channels opened by cAMP. The magnitude of the Cl current depended on the strength of Ca buffering in the bath solution, suggesting that the CNG and Cl channels were probably not organized as constituents of a local transducisome complex. Likewise, Cl channels and the Na/Ca exchanger, which extrudes Ca^{2+}, appear to be spatially segregated. Based on the theory of buffered Ca^{2+} diffusion, we determined the Ca^{2+} diffusion coefficient and calculated that the CNG and Cl channel densities on the membrane were ~8 and 62 μm^{-2}, respectively. These densities, together with the Ca^{2+} diffusion coefficient, demonstrate that a given Cl channel is activated by Ca^{2+} originating from multiple CNG channels, thus allowing low-noise amplification of the olfactory receptor current.

KEY WORDS: olfaction • signal transduction • Ca diffusion • ion channel

INTRODUCTION

Sensory transduction in vertebrate olfactory receptor neurons (ORNs) begins with the activation of specific receptor proteins on the plasma membrane of the cells' cilia by odorant molecules, leading via a G protein to stimulation of adenylyl cyclase to increase cAMP synthesis (for reviews see Schild and Restrepo, 1998; Gold, 1999). The rise in cAMP opens cyclic nucleotide–gated (CNG) channels that are permeable to both monovalent and divalent cations (Kurahashi and Shibuya, 1990; Zufall and Firestein, 1993; Dzeja et al., 1999). Consequently, Ca^{2+} in the ciliary cytoplasm increases (Leinders-Zufall et al., 1998; Reisert and Matthews, 2001b) and opens Ca-activated Cl channels. Because the Cl equilibrium potential across the ciliary membrane is much more positive than the resting membrane potential of ORNs (Zhainazarov and Ache, 1995; Reuter et al., 1998; Kaneko et al., 2001), a Cl efflux ensues, thus depolarizing the cell. This unusual, excitatory Cl current has been demonstrated in ORNs from amphibia (Kleene and Gesteland, 1991; Kurahashi and Yau, 1993), mammals (Lowe and Gold, 1993), and fish (Sato and Suzuki, 2000). Intracellular Ca^{2+} itself is regulated by a Na/Ca exchanger, which utilizes the inward-directed electrochemical Na gradient across the ciliary membrane to extrude Ca^{2+}, thereby restoring the basal intracellular Ca^{2+} concentration within a few seconds after the stimulus (Reisert and Matthews, 1998). In amphibians, the Cl channel is thought to serve as a safeguard of olfactory transduction by compensating for any decrease in transduction efficacy caused by dilution of the nasal mucus by fresh water (Kurahashi and Yau, 1993). When it was found to be present also in rat ORNs, a land-based mammal, the idea was proposed that this channel has evolved to serve conveniently as an amplifier of olfactory transduction (Lowe and Gold, 1993). Some general properties of this channel, including its activation caused by Ca^{2+} influx through the CNG channel, have been characterized in a frog excised-cilium preparation (Kleene, 1993). However, little is known about this channel in mammalian ORNs, despite its critical role in olfactory transduction. In the first part of this paper, we describe general properties of this channel in rat ORNs.

Address correspondence to Johannes Reisert, Department of Neuroscience, PCTB 906, Johns Hopkins University School of Medicine, 725 N. Wolfe St., Baltimore, MD 21205. Fax: (410) 614 3579; email: jreisert@jhmi.edu

*Abbreviations used in this paper: CaM, calmodulin; CNG, cyclic nucleotide–gated; ORN, olfactory receptor neurons.

J. Gen. Physiol. © The Rockefeller University Press • 0022-1295/2003/09/349/15 $8.00
Volume 122 September 2003 349–363
http://www.jgp.org/cgi/doi/10.1085/jgp.200308888

In the second part of the paper, we use these obtained properties of the Cl channel to investigate the functional relation between the Cl channel, the CNG channel and the Na Ca exchanger. A wide variety of neuronal functions depend on the interplay between Ca^{2+} influx through Ca-permeable ion channels and proteins controlled by intracellular Ca^{2+}. Based largely on studies of neuronal exocytosis (Neher, 1998; Meinrenken et al., 2003), it now appears that a network of sources and sinks of Ca^{2+} act together to establish a complex, dynamic profile of Ca^{2+} concentration on the cytoplasmic surface of the plasma membrane. Thus, the activation of Ca-gated ion channels can be understood from the spatial distribution of these channels within such a Ca profile. Decisive parameters for this functional coupling are the distances between Ca sources, Ca sinks, and the Ca-activated channels, as well as the speed of Ca^{2+} diffusion and the concentrations of Ca buffers. Since intracellular Ca^{2+} stores do not contribute to Ca^{2+} homeostasis in olfactory cilia (Zufall et al., 2000), and because the CNG channels, the Ca-activated Cl channel, and the Na Ca exchanger are all situated on the plasma membrane, it is possible to examine their functional interactions in a highly reduced system consisting of an inside-out membrane patch excised from rat ORNs. We introduce a method that can generally be applied to determine the distance between neighboring Ca-permeable channels and Ca-activated channels, and provides an estimate of channel densities in excised membrane patches. Recently, it has been suggested that olfactory transduction may take place in microdomains through supramolecular protein complexes (Schreiber et al., 2000; Goldstein et al., 2003). Our results, however, suggest that the Cl channel is not organized into a transduction complex with the CNG channel or the Na/Ca exchanger.

MATERIALS AND METHODS

Tissue Preparation

ORNs were isolated from female 4–10 wk old Wistar rats. The animal was decapitated after an overdose of isofluran in accordance with legally approved procedures and the head was split along the septum to expose the olfactory turbinates. Septal tissue and turbinates were transferred to extracellular solution and the tissue was separated from remaining cartilage. To aid dissociation, the tissue was incubated in extracellular solution (Table I) containing 0.2mg/ml trypsin (Sigma-Aldrich) for 30 min at 37°C and transferred to DNase solution (Table I). After gentle trituration, 0.5 ml of cell suspension was transferred to a recording chamber mounted on an inverted microscope with phase-contrast optics, and allowed to settle for 30 min before being continuously superfused with LiCl or NaCl solution.

Electrophysiological Recordings

Inside-out patches were excised from the dendritic knob of ORNs, which were easily recognized by their morphology. Cilia were often visible and were sometimes sucked into the tip of the recording pipette before a gigaohm seal was established. Therefore, the excised patches contained not only apical membrane of the dendritic knob, but also ciliary membrane. Pipettes were pulled from standard-wall borosilicate glass (Warner Instrument Corp.) and fire-polished to give an open-pipette resistance of 6–7 MΩ. Currents were recorded using an Axopatch-1D amplifier and acquired using a Digidata interface and pClamp software (Axon Instruments, Inc.). Junction potentials arising from dissimilar pipette and bath solutions were compensated. All data were sampled at 500 Hz and low-pass filtered (8-pole Bessel) at 100 Hz, with the exception of the noise recordings, which were digitized at 5 kHz, low-pass-filtered (8-pole Bessel) at 2.5 kHz, and subsequently digitally high-pass filtered at 2 Hz before variance calculations were made. Unless noted otherwise, the holding potential was −40 mV.

TABLE I

Solutions

	NaCl	KCl	LiCl	CholCl	NaF	$CaCl_2$	$MgCl_2$	$BaCl_2$	$SrCl_2$	HEDTA	EGTA
	mM	*mM*	*mM*	*mM*	*mM*	*mM*	*mM*	*mM*	*mM*	*mM*	*mM*
Extracell. sol.	125	5									10
DNase sol.	140						2				2
LiCl sol.			140							10	
NaCl sol.	140									10	
KCl sol.		140								10	
CholCl sol.				140							
0.25 μM Ca^{2+}			140			1.242				10	
0.75 μM Ca^{2+}			140			3.209				10	
2.4 μM Ca^{2+}			140			5.866				10	
11 μM Ca^{2+}			140			8.263				10	
67 μM Ca^{2+}			140			9.98				10	
1 mM Ca^{2+}			140			2					1
1 mM Mg^{2+}			140				1.03				1
1 mM Ba^{2+}			140					1.09			1
1 mM Sr^{2+}			140						1.09		1
F^- pipette sol.	10				130					10	

For current-voltage relations, care was taken not to introduce an artificial rectification due to the inactivation/desensitization of the Cl channel. For this purpose, patches were preexposed to 67 μM Ca^{2+} for 4 s to allow the current to partially inactivate. Thereafter, a double voltage ramp was used from −60 to +60 mV and then back to −60 mV at ±120 mV/s, and the two current-voltage relations were averaged. Leak currents in the respective Ca^{2+}-free solution were subtracted. Dose–response relations for the Ca-activated Cl conductance were constructed by normalizing individual patches to their maximal current in order to average data across patches. Subsequently, Hill functions were fitted to the collected data using Origin software (Microcal Software Inc., Northamptom, MA USA). Relative halide permeabilities and theoretical reversal potentials were calculated using the Goldman-Hodgkin-Katz equation. In calculations, the 9.98 mM $CaCl_2$ added to achieve 67 μM free Ca^{2+} were taken into account. Averaged values are mean ± SEM if not noted otherwise.

Solutions

All solutions contained 10 mM HEPES, with the pH adjusted to 7.2 with NMDG. DNase solution contained 0.2 or 0.4 mg/ml DNase 1 (Roche Diagnostics GmbH). The program Chelator (T.J.M. Schoenmakers, University of Nijmegen, Nijmegen, the Netherlands) or WinMAXC (C. Patton, Stanford University, Palo Alto, CA USA) was used to calculate free divalent concentrations in buffered solutions. The free Ca^{2+} concentrations in the HEDTA-buffered Ca solutions were determined using Ca-sensitive electrodes (Kennedy and Thomas, 1996). These solutions contained slightly different amounts of Cl^- because varied amounts of $CaCl_2$ were added to the buffered Ca solutions to obtain different free Ca^{2+} concentrations.

Whenever possible, Li^+ was used instead of Na^+ as the monovalent cation. Li^+ is permeant through the rat CNG channel (Frings et al., 1992) but does not support Na/Ca exchange (Reuter and Seitz, 1968; Reisert and Matthews, 1998), a mechanism that can potentially change the free Ca^{2+} concentration even in excised patches (see Fig. 8).

Rapid solution exchanges were achieved by transferring the pipette across the interface between neighboring solution streams using a system based on the Perfusion Fast-Step SF-77B (Warner Instrument Corp.). Solution exchange was complete within 15 ms.

Buffered Ca^{2+} diffusion

In the presence of excess HEDTA compared with Ca^{2+}, the free Ca^{2+} concentration at distance r from a Ca channel is linearly proportional to the Ca^{2+} flux, Φ (in number of Ca^{2+}/s), through this channel (Neher, 1986; Bauer, 2001).

$$[Ca^{2+}]_{free}^{local}(r) = \frac{\Phi}{2\pi N_{Av}(D_{Ca} + \kappa D_{HEDTA})} \cdot \frac{1}{r}\left(1 + \kappa \cdot \frac{D_{HEDTA}}{D_{Ca}} \cdot e^{-r \cdot \sqrt{\mu}}\right) + [Ca^{2+}]_0, \quad (1)$$

where N_{Av} is the Avogadro number, D_{HEDTA} and D_{Ca} the diffusion coefficients for HEDTA and Ca^{2+}, respectively, and

$$\mu = \frac{1}{\tau D_{HEDTA}} + \frac{\kappa}{\tau D_{Ca}},$$

with the reciprocal reaction time, τ^{-1}, for binding of Ca^{2+} to HEDTA at the basal-free Ca^{2+} concentration $[Ca^{2+}]_0$ being:

$$\tau^{-1} = k_{on} \cdot (k_{diss} + [Ca^{2+}]_0),$$

and the Ca^{2+}-binding ratio, κ, being:

$$\kappa = \frac{\partial[Ca^{2+}HEDTA]}{\partial[Ca^{2+}]} = \frac{K_{diss} \cdot [HEDTA]_{tot}}{(K_{diss} + [Ca^{2+}]_0)^2}.$$

In the latter equations, K_{diss} and k_{on} signify the thermodynamic equilibrium constant and the rate constant for Ca^{2+} binding to HEDTA, respectively. In our experiment, $[Ca^{2+}]_o = \sim 0$. Owing to the linear relation between $[Ca^{2+}]_{free}^{local}$ and Φ, the $[Ca^{2+}]_{free}$ due to the activation of several CNG channels can be calculated by summing $[Ca^{2+}]_{free}$ contributed by individual CNG channels, or

$$[Ca^{2+}]_{free}^{calc} = \sum n_i \cdot [Ca^{2+}]_{free}^{local}(r_i), \quad (2)$$

where $[Ca^{2+}]_{free}^{local}$ is from Eq. 1 and r_i and n_i denote the distance and number of CNG channels equidistant from the Cl channel in question. We calculate $[Ca^{2+}]_{free}^{local}$ using k_{on} = 4.5 $(\mu M \cdot s)^{-1}$, K_{Ca} = 4.47 μM (Naraghi and Neher, 1997), and D_{HEDTA} = 280 $\mu m^2/s$ (Allbritton et al., 1992). Based on a regular matrix of channels (Fig. 7 B), the r_i and n_i of the 15 nearest CNG channels of a given Cl channel are (in vector notation):

$$\{r_i\} = r_1 \cdot \{1; \sqrt{5}; 3; \sqrt{13}; \sqrt{17}; 5; \sqrt{29}; \sqrt{37}\} \text{ and } \{n_i\} = \{1; 2; 1; 2; 2; 3; 2; 2\}, \quad (3)$$

where r_1 denotes the distance between a given Cl channel and the closest CNG channel (Fig. 7 B). We then plot the difference ($\Delta[Ca^{2+}]$) between $[Ca^{2+}]_{free}^{calc}(r_1)$ and $[Ca^{2+}]_{free}^{exp}$, the local free Ca^{2+} concentration derived from the measured Cl current, as a function of r_1. The appropriate values for r_1 and D_{Ca} were chosen such that the zero-crossovers (the roots) of the following equations:

$$\Delta[Ca^{2+}]_{1HEDTA}(r_1) = [Ca^{2+}]_{1HEDTA}^{exp} - [Ca^{2+}]_{1HEDTA}^{calc}(r_1) \quad (4)$$

$$\Delta[Ca^{2+}]_{0.2HEDTA}(r_1) = [Ca^{2+}]_{0.2HEDTA}^{calc}(r_1) - [Ca^{2+}]_{0.2HEDTA}^{exp} \quad (5)$$

occur at the same r_1. Subscripts indicate HEDTA concentrations in mM. Note that Eqs. 4 and 5 are defined to have opposite signs and are, therefore, mirrored functions to facilitate accurate determinations of r_1 and D_{Ca}.

RESULTS

Run-down of the Ca-activated Cl Current in Excised Patches

We studied the Ca-activated Cl current with patch-clamp recording from inside-out membrane patches excised from the dendritic knob/cilia of rat ORNs (see MATERIALS AND METHODS). Although Cl channels and CNG channels are both present in the membrane, each channel population could be selectively activated by Ca^{2+} or cAMP in the bath solution. In most experiments, the pipette and bath solutions both contained LiCl instead of NaCl in order to disable the Na/Ca exchanger, which cannot be driven by Li^+ (Reuter and Seitz, 1968; Reisert and Matthews, 1998), so that the Ca^{2+} concentration near the membrane patch could be properly controlled by the bath solution. At −40 mV and with symmetrical 140 mM LiCl base solutions (no

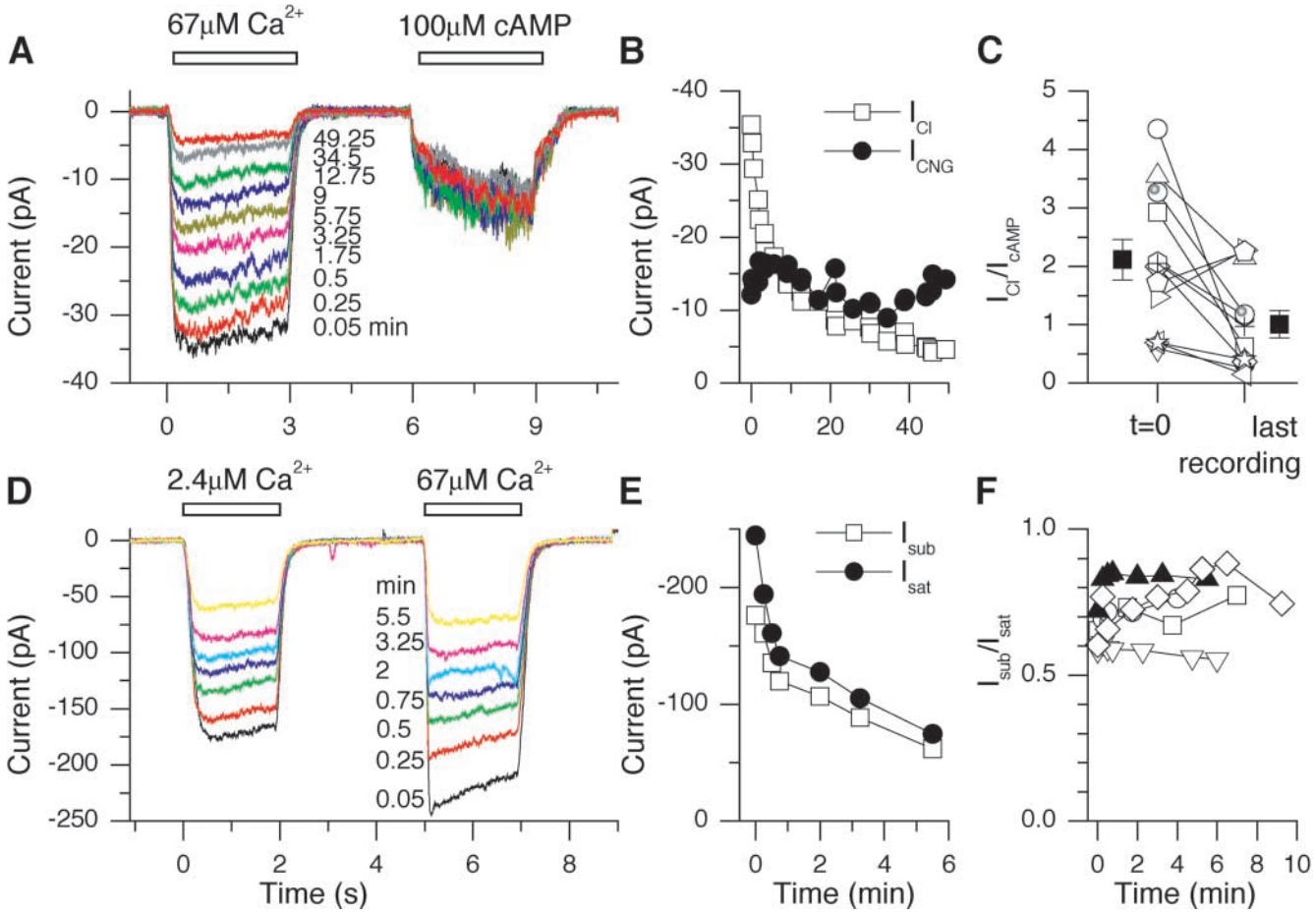

FIGURE 1. Run-down of the Ca-activated Cl current in excised patches. (A) Immediately after excision, an inside-out patch comprising membrane from the dendritic knob (and often cilia) was exposed for 3 s to saturating concentrations of Ca^{2+} (67 μM) and cAMP (100 μM) consecutively to induce maximal activation of Ca-activated Cl current and CNG current, respectively. The patch was held at −40 mV in symmetrical LiCl solutions. Repeated applications of the double-pulse protocol produced a gradual decline of the Ca-activated Cl current ("run-down"), whereas the CNG current remained constant. The time next to each trace denotes the beginning of each sweep after patch excision. (B) The maximal Ca-activated Cl and CNG currents from A are plotted against time after patch excision. (C) Individual patches showed a different degree of current run-down. Each open symbol represents one patch. On average, the current ratio, I_{Cl}/I_{CNG}, decreased from 2.11 ± 0.35 to 1.01 ± 0.23 (12 patches, ■, mean ± SEM). (D) Run-down of Ca-activated Cl current at both sub-saturating (2.4 μM) and saturating (67 μM) Ca^{2+} concentrations. (E) Similar time courses of Cl current run-down at sub-saturating and saturating Ca^{2+} concentrations. Data from D. (F) The ratio of sub-saturating to saturating currents, I_{sub}/I_{sat}, remained constant during run-down (5 patches; ▲ is the patch in D and E), demonstrating that the current run-down was not associated with a quantitative change in sensitivity to Ca^{2+}.

Ca^{2+} or Mg^{2+}; see Table I), application of 67 μM Ca^{2+} or 100 μM cAMP elicited a respective saturated current (Fig. 1 A), with the Ca-activated current initially being larger (83 ± 35 pA; 12 patches) than the cAMP-activated current (52 ± 18 pA; same 12 patches). It will be confirmed below that the Ca-activated current was indeed carried by Cl^-. In the course of time, this Ca-activated Cl current declined in amplitude, whereas the cAMP-activated current stayed quite constant (Fig. 1 B). This irreversible run-down of the Cl current, not hitherto described by others (Kleene and Gesteland, 1991; Hallani et al., 1998), occurred in most patches (10 of 12) and could be substantial. On average, the I_{Cl}/I_{CNG} ratio decreased from 2.11 ± 0.35 to 1.01 ± 0.23 (Fig. 1 C; 12 patches). The time course of run-down varied greatly between patches, ranging from a few minutes to almost an hour.

During current run-down, the quantitative sensitivity of the Cl channel to Ca^{2+} did not change, in that the ratio, I_{sub}/I_{sat}, of the currents elicited by a sub-saturating (2.4 μM) and a saturating (67 μM) Ca^{2+} concentrations remained constant over time (Fig. 1, D–F; five patches in F). Thus, the run-down appeared to reflect a progressive loss of functional Cl channels. This conclusion was supported by noise measurements to be described below.

The run-down of the Cl current was often biphasic. In the first few minutes after excision of the patch, the

current declined fairly quickly but thereafter the decline slowed down significantly (see, for example, Figs. 1 E and 5 B). Once the rapid phase of decline was over, experiments requiring relative current stability over an extended time period could be performed. All experiments described below were performed after the initial run-down.

Ionic Nature of the Ca-activated Current

To confirm that the Ca-activated current was indeed carried by Cl^-, we maintained the pipette Cl^- concentration ($[Cl^-]_o$) at 140 mM (Na salt) and progressively reduced the bath Cl^- concentration ($[Cl^-]_i$) by equimolar substitution with methanesulfonate (Na salt), an anion that does not permeate well through most Cl channels (for review see Frings et al., 2000). Current was activated by 67 μM Ca^{2+} in the bath. As $[Cl^-]_i$ was reduced, the reversal potential of the current-voltage relation shifted to negative values (Fig. 2 A) in a manner predicted fairly well by the Nernst equation (Fig. 2 B, mean ± SD from 9 patches), indicating that the channel was anion selective. The nonperfect Nernstian behavior could be due to methanesulfonate being slightly permeant through the channel. With equimolar replacement of bath NaCl by NaBr or NaI (NaCl in the pipette), and corresponding activation by 67 μM Ca^{2+} (see MATERIALS AND METHODS), the reversal potential shifted positively (Fig. 2 C), indicating that Br^- and I^- were more permeant than Cl^-. For the anion F^-, because CaF_2 is insoluble, the F^- permeability was tested with F^- in the pipette and Cl^- in the bath instead (inset in Fig. 2 C). From the reversal potential values and the Goldman-Hodgkin-Katz equation, the permeability sequence was $I^- > Br^- > Cl^- > F^-$ and the permeability ratios, P_x/P_{Cl}, were 3.23:1.98:1:0.16 (10 patches for Br^- and I^-, 6 patches for F^-). This sequence indicates that the relative permeability is inversely related to the hydration energy of the halide (Fig. 2 D).

We also tested the ability of divalent cations other than Ca^{2+} to activate the Cl channel. At −40 mV and 1 mM of each tested divalent cation, Sr^{2+} was quite effective (current ratio $I_{Sr}/I_{Ca} = 0.78$), Ba^{2+} was very ineffective ($I_{Ba}/I_{Ca} = 0.015$) and Mg^{2+} was completely ineffective (Fig. 2 E, F). Additional six patches exposed to 2 mM Mg^{2+} at 40 mV also produced no current. Therefore, it can be safely assumed that Mg^{2+} does not play a physiological role in the activation of these channels. Unless indicated otherwise, all subsequent experiments were performed in the absence of bath Mg^{2+}.

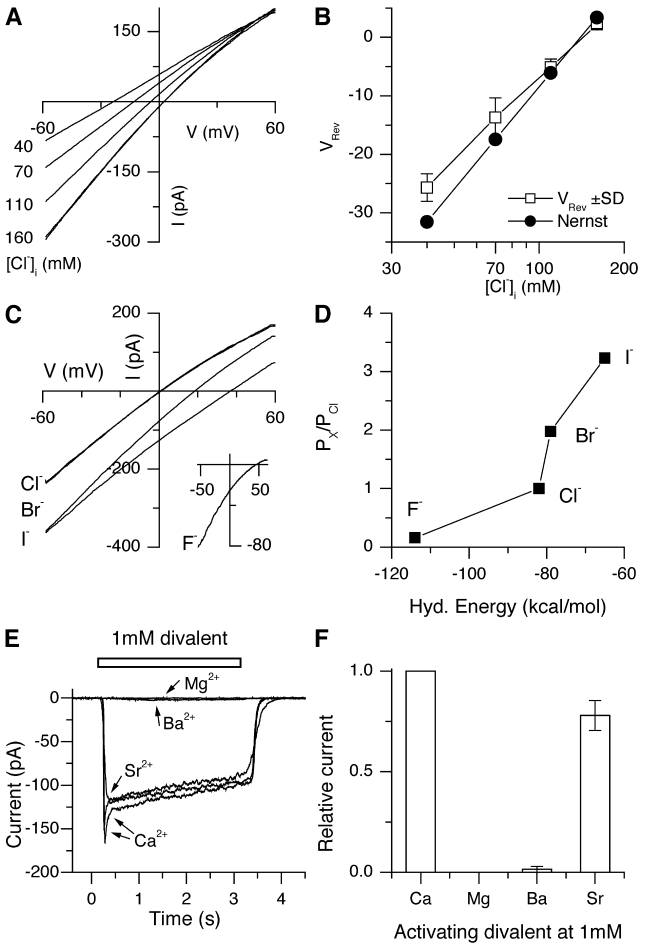

FIGURE 2. Anion selectivity of Ca-activated Cl current and its sensitivity to other divalent cations. (A) Current-voltage relation from an inside-out patch at 67 μM Ca^{2+} and the effect of replacing bath NaCl with equimolar Na-methanesulfonate. Numbers next to the traces indicate NaCl concentration in mM. Pipette solution contained NaCl. The trace labeled "160" actually represents two hardly distinguishable I-V curves, obtained at the beginning and the end of the experiment, respectively. (B) The dependence of the measured reversal potential (V_{Rev}) on $[Cl^-]_i$ (□) shows only a small deviation from the Nernstian prediction (●). Mean ± SD from nine patches. (C) Current-voltage relations from an inside-out patch at 67 μM Ca^{2+} with bath solution containing 140 mM Cl^-, Br^- or I^-. The trace labeled "Cl^-" actually comprises two literally identical I-V relations obtained at the beginning and the end of the experiment. The F^- permeability was measured separately in an inside-out patch (inset) with 140 mM F^- in the pipette solution and 140 mM NaCl solution and 67 μM Ca^{2+} in the bath solution. (D) Relative permeabilities (P_x/P_{Cl}) plotted against the hydration energy of each halide. Average of 10 (Cl^-, Br^- and I^-) and 6 (F^-) patches, respectively. (E) Exposure of an inside-out patch to four different divalent cations at 1 mM for 3 s. (F) Currents activated by divalent cations were normalized to the Ca-activated Cl current. Besides Ca^{2+}, only Sr^{2+} effectively activated the Cl^- channels. Mean ± SD of six patches.

Inactivation/Desensitization of the Ca-activated Cl Current

In addition to run-down, there was a reversible reduction of the current with a time course of seconds after activation by Ca^{2+} (see Fig. 1, 3, 4, 5). This reduction, which we refer to as inactivation/desensitization, also has not been described previously by others. Like the rundown, it did not show clear dependence on Ca^{2+}

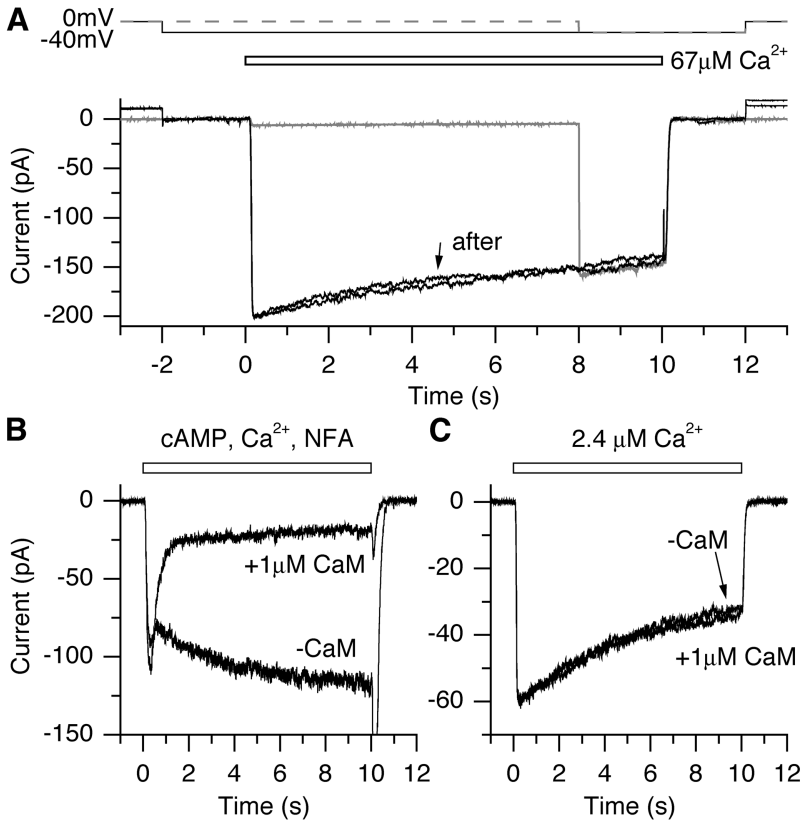

FIGURE 3. Inactivation/desensitization of Ca-activated Cl current. (A) Inactivation/desensitization depended on the presence of Ca^{2+}, but not on current flow through Cl channels. The current recorded at −40 mV during a saturating Ca^{2+} step showed the typical inactivation (black trace). Applying the Ca^{2+} step at 0 mV (near the Cl^- reversal voltage) induced no current, but inactivation proceeded at the same rate (gray trace). Repeating the step at −40 mV completely restored the original current ("after" trace). This experiment illustrates that inactivation is reversible and not associated with Cl^- permeation or Cl^- depletion. (B) CNG-gated channels are inactivated by Ca^{2+}-CaM. A patch was exposed to 10 μM cAMP and 67 μM Ca^{2+} (and 300 μM niflumic acid to block the Cl current) before and during application of CaM. 1 μM CaM quickly inactivated the cAMP-gated current. Holding potential was −40 mV. (C) Ca^{2+}-CaM did not alter the Ca-activated Cl current. Subsaturating Ca^{2+} steps at −40 mV induced currents with similar amplitude and time course in the presence or absence of CaM. Different patch from B.

concentration or membrane potential (see Fig. 4). It occurred regardless of whether Cl^-, Br^-, or I^- was the charge carrier (data not shown). The time course of current decline did not fit a single-exponential decline, and was not analyzed further in this work. This current decline could reflect the development of an inactivated/desensitized state of the Cl channel after Ca^{2+} binding, or result from current flow causing local depletion/accumulation of Cl^- (Zimmerman et al., 1988; Lindemann, 2001). We ruled out the second possibility by momentarily curtailing current flow to near zero by holding the membrane potential at zero. In such an experiment, we found that the current amplitude at a fixed time after Ca^{2+} exposure stayed the same regardless of how long the Cl current had been flowing (Fig. 3 A; experiment was performed in eight patches). Thus, the inactivation/desensitization appeared to be an intrinsic property of the channel itself.

Because calmodulin (CaM) is known to mediate multiple Ca-induced mechanisms of feedback inhibition in ORNs, we asked whether this protein also affected the inactivation/desensitization. In an excised patch, as expected from previous work (Chen and Yau, 1994; Bradley et al., 2001), the CNG current activated by a subsaturating (10 μM) cAMP concentration was reversibly inhibited by Ca^{2+}-CaM; 300 μM niflumic acid was present throughout in order to remove most of the Cl current (compare "-CaM" and "1 μM CaM" traces in Fig. 3 B). On the other hand, the Cl current activated by a subsaturating, buffered Ca^{2+} concentration (2.4 μM) was not affected by CaM (Fig. 3 C). At the same time, the drop in the current (i.e., inactivation/desensitization) was unchanged in the presence of CaM. The choice of a subsaturating Ca^{2+} concentration here was deliberate, in order not to overlook a mere shift in the Ca^{2+} concentration dependence of the current due to CaM. Similar results were obtained from seven patches. Thus, the inactivation/desensitization of the Cl current was neither caused by CaM nor sensitive to it. Possibly, it resulted directly from Ca^{2+} binding to the channel.

Dose–response Relation of the Ca-activated Cl Channel

To quantify the functional interaction between the Ca-activated Cl channel and the CNG channel, it is necessary to characterize the full dose–response relation between the Cl current and Ca^{2+} concentration. These experiments were performed after the rapid phase of the run-down was complete—a justifiable protocol because, as pointed out earlier, the run-down did not affect the quantitative dependence of the Cl channel on Ca^{2+} concentration. Only patches showing subsequent current run-down of <10% in the course of measurements were included for analysis. The Ca dependence was measured in symmetrical LiCl solutions and at ±40 mV (Fig. 4, A and C), using a Ca^{2+}-exposure time of 10 s. To test for

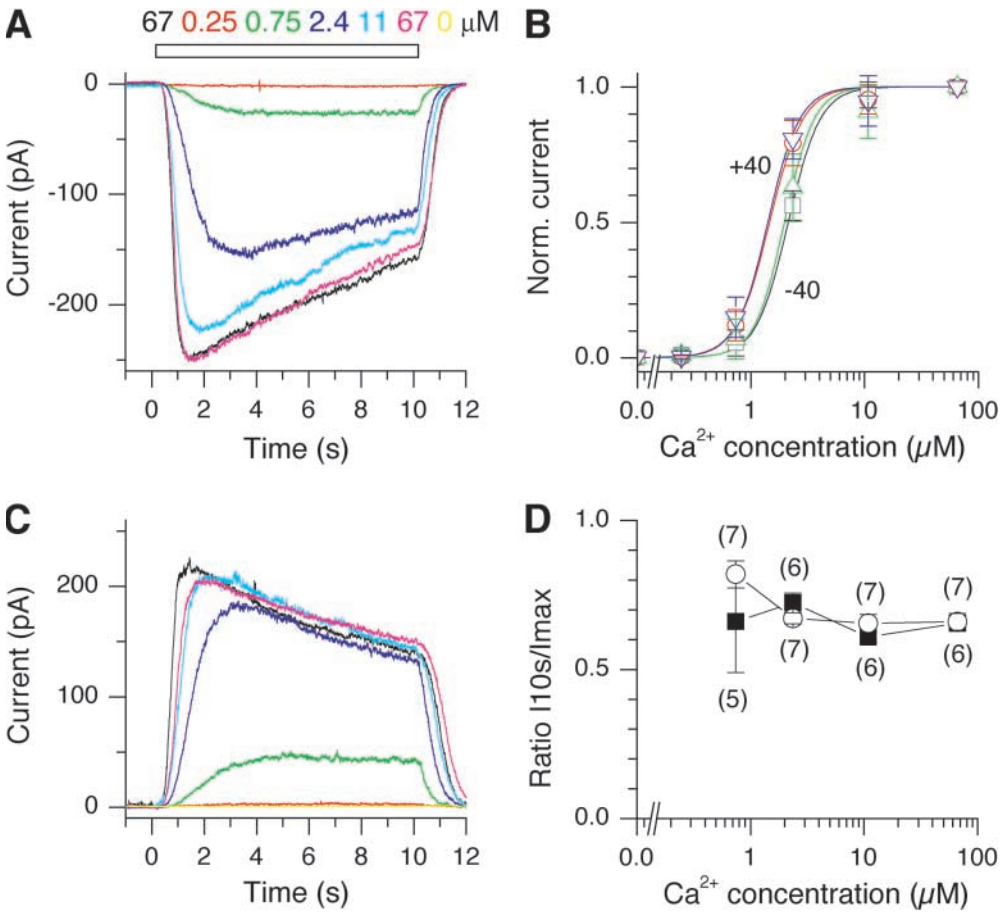

FIGURE 4. Quantitative dependence of Cl current on Ca^{2+}. (A and C) Cl current from an inside-out patch was activated by Ca^{2+} at increasing concentration at −40 mV (A) and +40 mV (C) after the rapid phase of the run-down was complete. Maximal currents recorded at the beginning (black traces) and at the end (magenta traces) had similar amplitudes, demonstrating stability of the Cl current (no further run-down) during the experiment. Upon application of Ca^{2+}, currents rose to a peak value and, thereafter, declined steadily. (B) Dose–response relations at +40 mV and −40 mV. At each voltage, the relations measured at the initial peak and at 10 s are almost indistinguishable. Data points show the mean ± SD of six patches at −40 mV and seven patches at +40 mV, normalized before averaging. Smooth curves are the Hill equation fitted to the data (see text for values). (D) The ratio of Cl current at 10 s versus transient peak is plotted as a function of the Ca^{2+} concentration at −40 mV (■) and +40 mV (○). The ~40% current reduction over 10 s was relatively constant over the applied Ca^{2+} concentration. Numbers of patches are indicated with each mean value.

any sensitivity change due to inactivation/desensitization, the current amplitudes at transient peak and at 10 s were both used for constructing dose–response relations (mean ± SD of normalized data shown in Fig. 4 B; −40 mV: six patches; +40 mV: seven patches). The smooth curves are Hill-equation fits. At –40 mV, the Ca^{2+} concentration for half-maximal activation, $K_{1/2}$, was 2.2 μM for peak current (black) and 2.1 μM for current at 10 s (green); the Hill coefficient, n, was 2.8 and 2.8, respectively. At +40 mV, the $K_{1/2}$ was 1.5 μM (red) and 1.4 μM (blue), and n was 3 and 3, respectively. Thus, like run-down, channel inactivation/desensitization was not associated with a quantitative change in the Ca sensitivity (see also Fig. 4 D). The slight decrease in $K_{1/2}$ at positive voltages could in principle reflect a voltage sensitivity in the Ca binding step or the gating step.

Ratio of Maximum Ca-activated Cl Current to Maximum CNG Current under Physiological Concentrations of External Divalent Cations

Monovalent current through CNG channels is sensitive to blockage by external divalent cations (Haynes et al., 1986; Zufall and Firestein, 1993; Frings et al., 1995; Dzeja et al., 1999). Thus, in order to compare the magnitudes of the CNG and Cl currents in the intact-cell situation, we included physiologically relevant concentrations of divalent cations (2 mM Ca^{2+}, 1 mM Mg^{2+}) in the pipette solution (Fig. 5 A). Under these conditions, the Cl current activated by a saturating concentration (67 μM) of Ca^{2+} shortly after patch excision remained large (136 ± 41 pA; 16 patches), but the CNG current elicited by a saturating concentration (100 μM) of cAMP was very small (4.4 ± 1.2 pA; 16 patches). As in the absence of divalent cations, the Cl current still showed run-down and inactivation/desensitization, whereas the cAMP-activated current remained constant throughout (Fig. 5 B). The mean initial current ratio I_{Cl}/I_{CNG} in this case was 33.34 ± 8.97 (indicated by ■ in Fig. 5 C; 16 patches), instead of just twofold in the absence of divalent cations (see above). Even after run-down, this ratio stayed at 22.54 ± 7.43. Thus, in physiological ionic conditions, the maximum Ca-activated Cl current was ~30-fold that of the cAMP-activated current.

Under the above experimental conditions, Ca^{2+} from the pipette will enter the patch through the CNG chan-

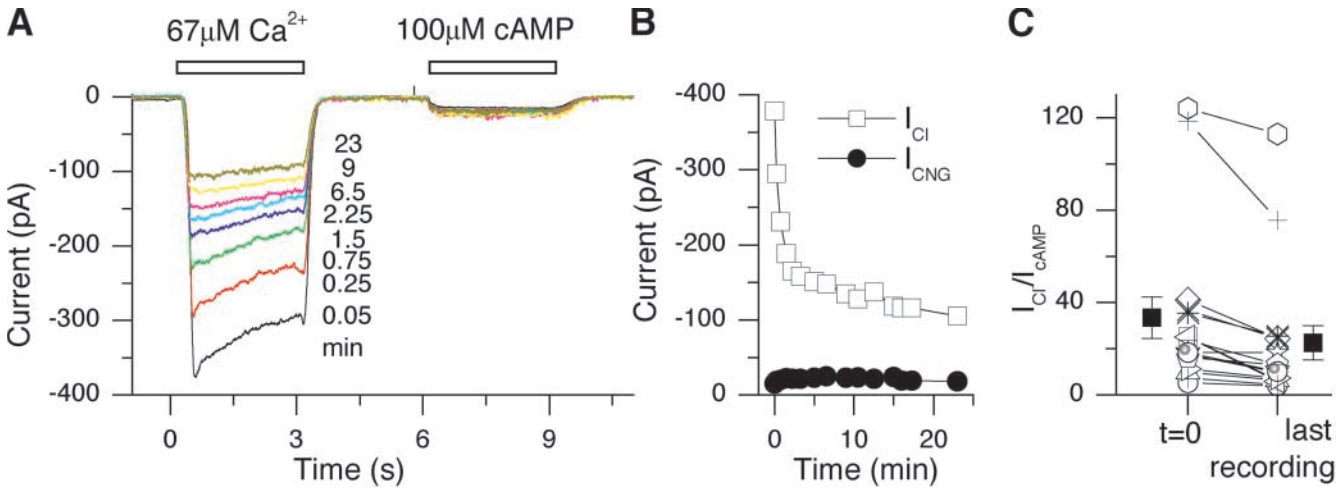

FIGURE 5. Relative magnitudes of Ca-activated Cl current and CNG current in the presence of external divalent cations. Same experiment as in Fig. 1, but with 2 mM Ca^{2+} and 1 mM Mg^{2+} in the pipette solution. (A) An inside-out patch was exposed for 3 s sequentially to 67 μM Ca^{2+} and 100 μM cAMP. Otherwise symmetrical LiCl solutions. Holding potential was −40 mV. The CNG current was strongly suppressed by external Ca^{2+} and Mg^{2+}, but the Ca-activated Cl current remained substantial. (B) Run-down of the Ca-activated Cl current persisted in the presence of external divalent cations, but the small CNG current stayed constant. (C) The mean ratio of Cl current to CNG current in the presence of external divalent cations was 33.34 ± 8.97 before Cl current run-down and 22.54 ± 7.43 (16 patches, ■, mean ± SEM) after run-down. Open symbols represent individual patches, with I_{Cl}/I_{CNG} ranging from 5.3 to 124.

nel during application of cAMP. This could potentially activate the Cl channel and generate an additional current component. However, with the high HEDTA concentration of 10 mM used, this was unlikely to happen (see Fig. 7).

Relative Cl and CNG Channel Numbers, and Single-channel Parameters

For the modeling to be described later, it is necessary to know the current through a single Cl channel and also the quantitative amount of Ca^{2+} influx through a single olfactory CNG channel. At least for the Cl channel, single-channel measurements are not feasible because the unitary current is too small. We therefore resorted to noise analysis. We took advantage of the fact that, in some patches, the membrane current developed slowly and decayed even more slowly despite rapid application/removal of 100 μM cAMP or 67 μM Ca^{2+}, presumably due to a slow exchange of solutions (Fig. 6, A and B). In the case of the Ca-activated Cl current, we deliberately slowed the Ca^{2+} washout further by using a bath solution containing a low concentration of Ca buffer (0.1 mM HEDTA) between Ca^{2+} exposures. When high-pass filtered at 2 Hz (Fig. 6, A and B, traces labeled "hi-pass"), an increase in noise was evident during the falling phases of the CNG and Cl currents, taken to originate from the more frequent transitions between the open and closed states of the channels at submaximal open probabilities. Assuming, for simplicity, a single open state and a single closed state, the increase in current variance (σ^2) is related to the unfiltered mean current (I) by the parabolic function $\sigma^2 = iI - I^2/N$, where i is the single-channel current and N is the total number of channels on the patch (DeFelice, 1981). This equation fits the data quite well for both the CNG channel (Fig. 6 C) and the Cl channel (Fig. 6 D, different patch). In the experiments shown, i = 0.49 pA and N = 385 for CNG channels, and i = 0.07 pA and N = 999 for Cl channels. The ratio of maximum current (see figure legend) to N * i gave a maximal open probability, P_o, of 0.83 for the CNG channel and near 1.0 for the Cl channel. From multiple experiments, the mean single-channel current at −40 mV was −0.49 ± 0.04 pA for the CNG channel (nine patches) and −0.051 ± 0.003 pA for the Cl channel (seven patches). The mean P_o was 0.8 for the CNG channel and 0.97 for the Cl channel. The ratio of channel numbers (i.e., N_{Cl}/N_{CNG}) was 3.6 ± 2.2.

Because the P_o value for the Cl channel remained near unity even though the measurements were made after the rapid run-down of the current, the run-down itself could not be due to a decrease in P_o. Thus, as for other ion channels (for review see Becq, 1996), run-down was most likely due to a loss of functional channels, a phenomenon that was also described for Ca-activated Cl channels in aortic smooth muscle cells (Hirakawa et al., 1999).

A similar ratio of Cl channel to CNG channel numbers can be derived in another way. In the absence of external divalent cations, and before Cl current run-down, the average I_{Cl}/I_{CNG} was ~2 in symmetrical LiCl solutions (Fig. 1 C). Because Li^+ carried current half as

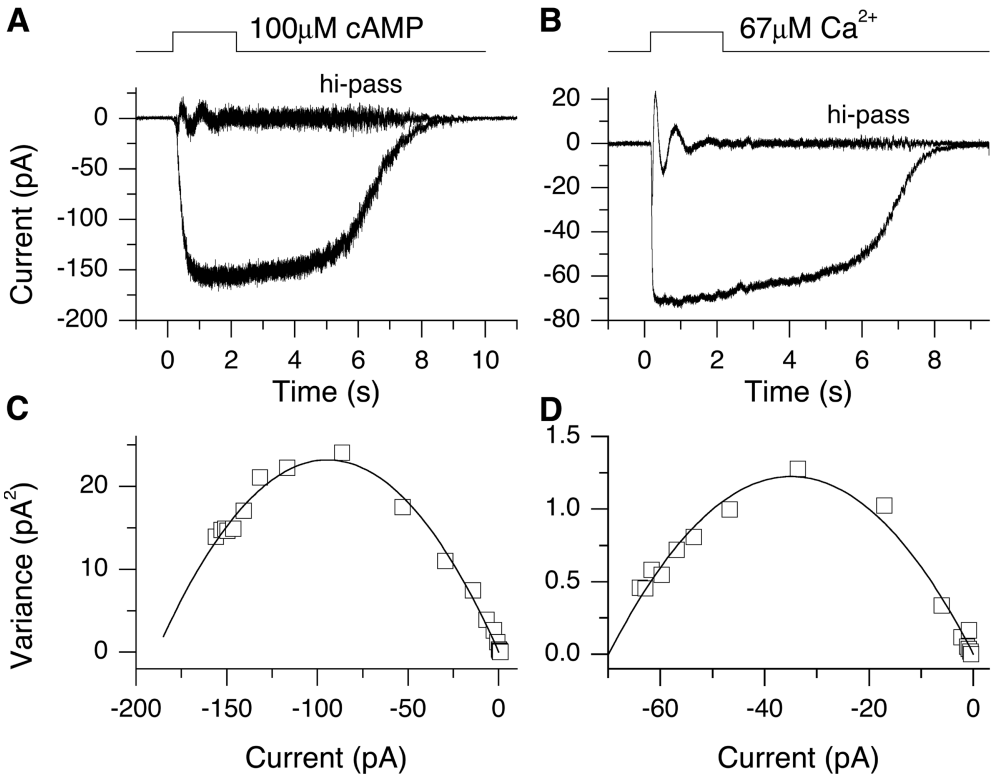

FIGURE 6. Extraction of unitary CNG and Ca-activated Cl currents from variance analysis. (A) An inside-out patch was exposed for 2 s to 100 μM cAMP in divalent-free symmetrical NaCl solution at −40 mV. The patch showed a slow decline in current after the removal of cAMP, probably because of poor solution exchange in the patch. High-pass filtering at f_c = 2 Hz (trace labeled "hi-pass") revealed an increased current variance during slow washout of cAMP, reflecting enhanced gating activity of channels at submaximal open probability (P_o). The sinusoidal waveform at the start of the trace is an artifact of the high-pass filtering. (B) A Ca-activated Cl current was recorded at −40 mV, which again was high-pass filtered at 2 Hz. Different patch from A. (C) Plot of variance against amplitude of the cAMP-activated current for data from A. The fitted parabolic function is $\sigma^2 = iI - I^2/N$ (see text), yielding N = 385 and i = 0.49 pA. (D) Variance analysis for the Ca-activated Cl channel in B. Fit parameters were N = 999 and i = 0.07 pA.

well as Na^+ through the olfactory CNG channel (Frings et al., 1992), the I_{Cl}/I_{CNG} ratio in symmetrical NaCl solutions would therefore have been near unity, i.e., $I_{Cl} = I_{CNG}$. The ratio of the respective channel numbers is $N_{Cl}/N_{CNG} = (i_{CNG} \times P_o^{CNG})/(i_{Cl} \times P_o^{Cl})$, where i_{Cl} and i_{CNG} are the average single-channel currents (see above). With the above values of P_o^{CNG} and P_o^{Cl}, we obtain N_{Cl}/N_{CNG} = 7.8. After run-down of the Cl current (see Fig. 1 C), this ratio would decrease to ~4. This value agrees quite well with the number of 3.6 derived above from noise analysis. Below, we adopt the value of 4 after run-down for modeling.

Functional Link between CNG Channels and Cl Channels

During the response to odorants, Cl channels are activated by Ca^{2+} that enters the ORN cilia through the CNG channels. Therefore, the distance between the Cl and CNG channels is key to Ca signaling in these neurons. Recently, it has been suggested that scaffolding proteins in olfactory cilia (Schreiber et al., 2000; Goldstein et al., 2003) organize components of olfactory transduction into a tranducisome complex as in *Drosophila* photoreceptors (for review see Tsunoda and Zuker, 1999). In a transducisome, intermolecular distances are in the range of <10 nm because the transduction molecules are immediate neighbors within the supramolecular complex (for review see Sheng and Sala, 2001). Ca^{2+} entering the cell via a CNG channel would travel this distance in such a short time that binding to a buffer is effectively impossible (Neher, 1998) and the secondary activation of the Cl channel should therefore be unaffected by changes in the Ca-buffer concentration. A test for proximity on the scale of a transducisome would be to examine whether the functional coupling between CNG channels and Cl channels can be intercepted with a Ca buffer (HEDTA). If coupling was not affected with HEDTA, the two channels would likely be very close together and possibly components of a transducisome. In the following, we show first that the coupling is indeed strongly affected by HEDTA, and second, that this finding can be used for estimating the mean distance between the two channel types on the membrane.

A patch was held in symmetrical CholCl solutions in order to suppress monovalent cation flux through the CNG channels (Balasubramanian et al., 1995). In addition, the pipette solution contained 1 mM Ca^{2+} to support Ca^{2+} flux through the CNG channels. In the experiment of Fig. 7 A, saturating (67 μM) Ca^{2+} in the bath elicited a peak current of −30 pA at −40 mV (black trace). With 100 μM cAMP and at high Ca-buffering capacity (1 mM HEDTA) in the bath solution, the Ca^{2+} flux from the pipette solution through the fully activated CNG channels induced only about −8 pA of

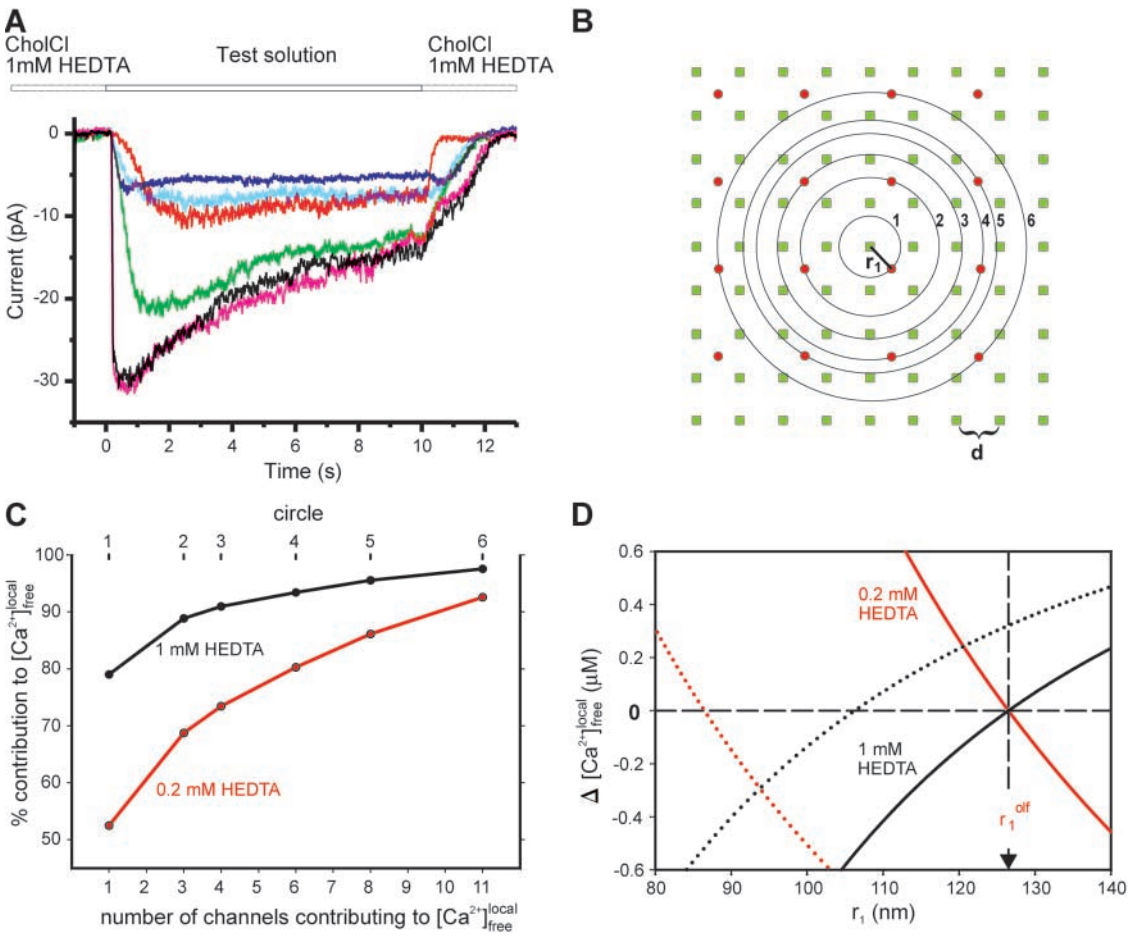

FIGURE 7. Functional interaction between Cl channel and CNG channel. (A) Ca^{2+} influx through CNG channels induced a Cl current in an inside-out patch. The pipette solution contained CholCl and 1 mM Ca^{2+}, and the holding potential was −40 mV. Application of a saturating (67 μM) Ca^{2+} concentration produced a maximal Ca-activated Cl current (black and magenta traces, representing the first and last traces in the experiment). At low Ca-buffer capacity (0.2 mM HEDTA), 100 μM cAMP caused sufficient Ca^{2+} influx to induce a steady activation of Ca-activated Cl current (green trace). Activation of Cl current to 70% of maximum indicates a steady local Ca^{2+} concentration of ~2 μM. The Cl current is completely suppressed by 300 μM niflumic acid (dark-blue trace). Increasing the Ca-buffer capacity to 1 mM HEDTA prevented the activation of Cl channels (light-blue trace). (B) Model for the spatial arrangement of Ca-activated Cl channels (green) and CNG channels (red) in the ciliary membrane. The 4:1 ratio of channels reflects the observation that 4-times more active Cl channels can be detected in excised patches after complete run-down. The symbol d denotes the spacing between Cl channels, and $r_1 = d/\sqrt{2}$ is the distance from a given Cl channel to the nearest CNG channel. The distances to the 11 nearest CNG channels considered for the local free Ca^{2+} concentration are marked $r_1 - r_6$. (C) Contribution of increasingly distant CNG channels to the local $[Ca^{2+}]^{calc}_{free}$ sensed by a Cl channel. The values r_1 and D_{Ca} obtained for a given number of channels were used to calculate $[Ca^{2+}]^{calc}_{free}$ and expressed as a percentage of $[Ca^{2+}]^{calc}_{free}$ calculated for 15 CNG channels. This panel illustrates that 11 CNG channels belong to the catchment area of a Cl channel at 0.2 mM HEDTA, and have to be considered as Ca^{2+} sources in the model. (D) Determination of distance r_1 between Cl channels and CNG channels. For 1 mM HEDTA the graph shows the difference between the experimentally determined and the calculated Ca^{2+} concentrations while for 0.2 mM HEDTA the same function only with opposite sign, the difference between the calculated and the experimentally determined $[Ca^{2+}]_{free}$ is shown. The use of mirrored functions facilitates the accurate determination of D_{Ca} such that both functions have the same zero-crossover, i.e., intersect exactly at the abscissa (see MATERIALS AND METHODS). This was achieved with r_1 = 126.5 nm and D_{Ca} = 89.5 $\mu m^2/s$ (solid lines), while with even a small deviation of D_{Ca} from this value the two curves do not have the same zero-crossover (dotted line is the cytosolic D_{Ca} of 220 $\mu m^2/s$, Allbritton et al., 1992). The experimentally determined $[Ca^{2+}]^{exp}_{free}$ were 2.65 and 1.1 μM at 0.2 and 1 mM HEDTA, respectively (average of eight patches).

current (Fig. 7 A, light-blue trace). With reduced bath Ca-buffer capacity (0.2 mM HEDTA), the current induced by cAMP increased to −21 pA (green trace). The cAMP-induced current was greatly suppressed by 300 μM niflumic acid (dark-blue trace), demonstrating that it was largely carried by Cl^-, plus a small fraction being carried by Ca^{2+} through the CNG channels. When a solution containing 0.2 mM HEDTA and no cAMP was applied (red trace) a smaller current was observed that probably originated from spontaneous gating of the CNG channel (Kleene, 2000) or from residual cAMP still present in the immediate vicinity of the

patch. As expected, when Ca^{2+} influx was largely minimized by clamping the membrane potential at 40 mV, no Cl current was observed (data not shown). The time course and extent of the Cl current decline (inactivation/desensitization) during the cAMP steps resembled those recorded during Ca pulses (compare Fig. 4), indicating that the local Ca profile sensed by the Cl channels already reached steady state during the cAMP step. The cAMP-induced Cl current thus illustrates a functional link between the CNG channels and the Cl channels. However, its sensitivity to a change in HEDTA concentration provides qualitative evidence against the notion that the two transduction channels are assembled within transducisomes. Previously, Kleene (1993) has likewise shown that the presence of BAPTA (a faster buffer than HEDTA) in an excised cilium could affect the Cl current activated by Ca^{2+} entering through the CNG channel.

How far are CNG channels and Cl channels separated? The average time required for Ca^{2+} to bind a buffer molecule depends on the binding rate and the buffer concentration. This time period determines the mean distance Ca^{2+} can freely diffuse from the CNG channel, which is, generally, 100–200 nm (Neher, 1998). Based on the theory of buffered Ca^{2+} diffusion (Neher, 1986; Bauer, 2001), we calculated the mean distance, r, between neighboring CNG and Cl channels using the above measurements. Each CNG channel constitutes a point source of Ca^{2+}, surrounded by a radially symmetrical Ca^{2+} concentration ($[Ca^{2+}]_{free}$) profile that peaks at the pore and decays with increasing distance from the channel. This concentration profile depends on the Ca^{2+} flux through a CNG channel, the binding to HEDTA, and the Ca^{2+} diffusion coefficient D_{Ca}. With more than one CNG channel around, the $[Ca^{2+}]_{free}$ profiles generated by individual channels in the presence of excess Ca buffer simply sum (see below and MATERIALS AND METHODS). The amplitude of the current through a Cl channel depended on its location within this summed Ca profile, and therefore on the distances between the CNG channels and the Cl channels. From our estimates of the single CNG channel current (0.49 pA) and its P_o (0.8), together with the previous finding that the macroscopic monovalent current is reduced to 16% in the presence of 1 mM external Ca^{2+}, of which the fractional current carried by Ca^{2+} is 0.4 (Dzeja et al., 1999), we calculated a Ca^{2+} current through a single CNG channel under our experimental conditions to be 0.025 pA, or 78,000 Ca^{2+}/s. Because the efficiency of Ca buffering by HEDTA is also known (Thomas, 1982; Naraghi and Neher, 1997), the remaining parameters, D_{Ca} and r, can be solved by experimentally measuring $[Ca^{2+}]_{free}^{exp}$ at two different HEDTA concentrations using the Cl channels as a Ca^{2+} sensor. The experiment described above provided the necessary measurements. Thus, at HEDTA concentrations of 1 mM and 0.2 mM, the average fractional activation of Cl channels was measured to be ~10% and ~58%, respectively, corresponding to local $[Ca^{2+}]_{free}^{exp}$ at the Cl channels of 1.1 ± 0.27 μM and 2.65 ± 0.21 μM (mean ± SD, eight patches) based on the dose–response relation of Fig. 4 B. The current activated upon application of cAMP represented a mixed current carried by Ca^{2+} and Cl^-. From this total current, the average fractional activation of Cl channels was calculated by subtracting the Ca current component, achieved as follows. Because the maximal Cl current was measured and the single Cl channel current had also been determined earlier, the number of Cl channels can be calculated, from which the number of CNG channels can be derived using the 4:1 ratio of Cl channels to CNG channels. The amount of Ca current could then be estimated with the above calculated single-channel current of 0.025 pA under the adopted experimental conditions.

Because the CNG channels and Cl channels appeared not to be clustered in transducisomes, we assumed that they are arranged in a regularly-spaced matrix (Fig. 7 B), with a ratio of four functional Cl channels per CNG channel after the fast run-down of the Cl current. This assumption allows to derive an analytical solution of the Ca diffusion problem (see MATERIALS AND METHODS). As mentioned above, the local $[Ca^{2+}]_{free}$ at a given Cl channel is equal to the sum of contributions from surrounding CNG channels, with decreasing contributions from more distant CNG channels (represented by concentric circles in Fig. 7 B). To quantify the contributions from distant channels, we fitted the measurements with the appropriate D_{Ca} and r values for the case of up to 15 CNG channels (circles 1–7 inclusive) contributing to the local $[Ca^{2+}]_{free}$ sensed by each Cl channel. We then repeated the calculations for decreasing numbers of circles and related the results to that obtained with 15 channels (=100% in Fig. 7 C) (it was not feasible to extend the model beyond 15 channels without taking into account the specific geometry of the patch; see below). The conclusion was that at least 11 channels (circles 1–6 in Fig. 7 B) had to be included in the model in order to account for >90% of $[Ca^{2+}]_{free}^{calc}$ at both 0.2 mM and 1 mM HEDTA (Fig. 7 C). With fewer channels included, the resulting values deviated by up to 50% from the reference value. The contributions from distant channels were especially obvious at the lower Ca-buffer capacity, reflecting the importance of long-range Ca^{2+} diffusion at low Ca-buffer concentrations. For the following calculations, we included the Ca influx through 11 CNG channels to the activation of each individual Cl channel.

In the matrix shown in Fig. 7 B, the distance r_1 between a Cl channel and the nearest CNG channel is re-

lated to the space constant, d, of the matrix by $r_1 = d/\sqrt{2}$. The other distances, such as r_2 and r_3, can likewise be expressed as functions of d, and therefore r_1. The values of r_1 and D_{Ca} were adjusted by successive reiterations so that the calculated $[Ca^{2+}]^{calc}_{free}$ values matched the $[Ca^{2+}]^{exp}_{free}$ values measured from the Cl currents for both 0.2 mM and 1 mM HEDTA conditions (Fig. 7 D). From eight patches, mean r_1 = 126.5 ± 41.7 nm (range 108–148 nm) and mean D_{Ca} = 89.5 ± 19.5 $\mu m^2/s$ (range 43–134 $\mu m^2/s$). The error bars were estimated by using the values of the upper and the lower bound of the SD of the local $[Ca^{2+}]^{exp}_{free}$ at the Cl channel (see above). The corresponding mean channel densities were 31 Cl channels and 8 CNG channels per μm^2. Since ~50% of the active channels were lost during rundown, the estimated mean densities in vivo would be 62 μm^{-2} for Cl channels and 8 μm^{-2} for CNG channels.

Excised from the dendritic knob, the membrane patches often contained one or more cilia. We have therefore recalculated r_1 and D_{Ca} using, instead of a planar model as in Fig. 7 B, a model consisting of a linear channel arrangement in order to simulate a long slender cilium. The derived r_1 value and channel densities remained similar to above, though D_{Ca} was reduced by a factor of 2 (data not shown). Nonetheless, the calculations indicated that, even in this case, each Cl channel still monitors Ca^{2+} originating from several CNG channels. Thus, regardless of patch geometry, the conclusion of a spatial integration of Ca signals from more than one CNG channel appears to hold.

Functional Link between Cl Channel and Na/Ca Exchanger

While the CNG channel is responsible for an increase in ciliary Ca^{2+} upon activation by odorants, a Na-dependent Ca extrusion returns Ca^{2+} to the basal level (Reisert and Matthews, 1998). We likewise asked whether the Na/Ca exchanger and the Cl channel are organized into transducisome-like complexes. To address this question, we ran the Na/Ca exchange in reverse mode in order for it to serve as a Ca^{2+} source for activating Cl channels in an excised patch, and asked whether the resulting Cl current was sensitive to Ca-buffering in the bath solution. In this experiment, the pipette solution contained 140 mM CholCl plus 2 mM Ca^{2+}. Reverse Na/Ca exchange was facilitated by holding the membrane potential at 40 mV, in order to take advantage of its electrogenicity (for review see Blaustein and Lederer, 1999). With initially 140 mM CholCl in the bath, maximal activation of Cl channels by saturating (67 μM) Ca^{2+} in the bath produced a current of 40 pA (Fig. 8, black trace). In the absence of bath Ca^{2+}, replacing the bath CholCl with NaCl elicited a steady-state current of ~20 pA at the low Ca-buffering capacity of 25 μM HEDTA (Fig. 8, red trace). This current was substantially reduced by 300 μM niflumic acid, thus identifying its Cl constituency (Fig. 8, green trace). The current was also absent when the internal HEDTA concentration was increased to 1 mM (dark-blue trace). The involvement of the Na Ca exchange in generating the Cl current was further supported by the fact that Li^+ was unable to substitute for Na^+ for generating the Cl current (Fig. 8; Na^+, red trace; Li^+, light-blue trace). Similar results were obtained from a total of six patches. In our experiments, reverse Na/Ca exchange was able to operate in the absence of K^+. Thus, the exchanger on olfactory cilia apparently does not depend on K^+ cotransport, unlike the Na/Ca,K-cotransporter in photoreceptors (Cervetto et al., 1989). This experiment suggests that the Cl channel and the Na/Ca exchanger are likewise situated in close proximity on the ciliary membrane, but far enough to allow interception of Ca^{2+} by Ca buffers. A quantitative estimate of the distances between the two, however, is not possible be-

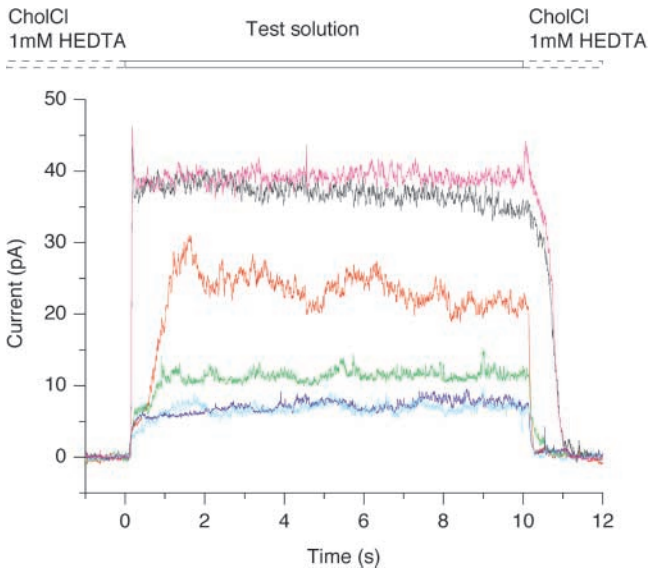

FIGURE 8. Functional interaction between Cl channel and Na/Ca exchanger. When driven in reverse mode, the Na/Ca exchanger transports Ca^{2+} from the external solution to the cytoplasmic face of the patch membrane, where Ca-dependent Cl channels were activated. The pipette contained CholCl and 2 mM Ca^{2+}, the holding potential was +40 mV. The maximal Ca-activated Cl current was determined by applying 67 μM Ca^{2+} (black and magenta traces, representing the first and last traces in the experiment) in CholCl solution. Upon replacing CholCl with NaCl (red trace, Ca-buffer capacity was reduced to 25 μM HEDTA), reverse Na/Ca exchange activated a constant Cl current that corresponded to 60% of the maximal current. This current was blocked by 300 μM niflumic acid (green trace) and did not occur at elevated Ca-buffer capacity (1 mM HEDTA, dark-blue trace). It also depended strictly on Na^+ and could not be generated by Li^+ (light-blue trace). A small pedestal-like current was observed when the solution was changed from $Chol^+$ to Na^+ or Li^+ -containing solution, the origin of which is not fully understood, but might originate from current through CNG channels open even in the absence of cAMP (Kleene, 2000).

cause there is currently no information about the density of the exchanger and its Ca-transport rate.

DISCUSSION

General Properties of Ca-activated Cl Channel

Previously, the olfactory Ca-activated Cl channel has been studied in frog (Kleene and Gesteland, 1991; Kleene, 1993, 1997). Generally speaking, the properties of the frog channel are similar to those of the rat channel. In both animal species, this channel shows inward rectification, a small single-channel conductance (0.5–1.5 pS), an activation $K_{1/2}$ of slightly over 2 μM Ca^{2+} at −40 mV, an open probability of the liganded channel near unity, and a lack of sensitivity to calmodulin (Kleene and Gesteland, 1991; Kleene, 1997, 1999). The dose–response relation displays pronounced cooperativity, suggesting that at least three Ca^{2+} ions must bind to open a channel, a mechanism that might contribute to the steep dependence of the odor-induced response on stimulus concentration (Firestein et al., 1993), especially in mammals (Reisert and Matthews, 2001a). The above lack of any major species-dependent differences we found is in contrast to the recent results of Hallani et al. (1998). This group also studied the rat channel on excised, inside-out membrane patches from the dendritic knob of ORN, but found a linear current-voltage relation and a $K_{1/2}$ value of 26 μM Ca^{2+} at an unspecified membrane potential. Because they used unbuffered Ca solutions, it is difficult to evaluate their results. Also, they found an unusual halide permeability sequence ($Cl^- > F^- > I^- > Br^-$), whereas the sequence we obtained ($I^- > Br^- > Cl^- > F^-$) is similar to those reported for Ca-activated Cl channels in other cell types (for review see Frings et al., 2000). Finally, they reported a strong current suppression at all voltages when Cl^- was replaced by other halides, which we did not observe.

The current run-down we observed was not described by Hallani et al. (1998) or in frog (Kleene and Gesteland, 1991; Kleene, 1993). In the latter case, the current run-down could have been missed because in these experiments Cl current activation occurred via diffusion of Ca^{2+} into an excised cilium, a relatively slow process. The run-down could arise from the elution of a soluble factor that is required for the gating of the channel by Ca^{2+}. In other tissues, a variety of modulators of Ca-activated Cl channels have been described or postulated. Protein kinases (CaMK II and PKC), inositol polyphosphates, and cytoskeletal proteins can affect the time course of Ca-activated Cl currents in epithelial and smooth-muscle cells (Ismailov et al., 1996; Schlenker and Fitz, 1996; Wang and Kotlikoff, 1997; Xie et al., 1998), although the details of these modulations are not understood. Whatever its mechanism, this run-down of the olfactory Cl current may contribute to the progressive reduction of the odor-induced receptor current recorded in the whole-cell configuration (e.g., Zhainazarov and Ache, 1995).

In contrast to the run-down, which is observed only for excised patches or dialyzed ORNs, the intrinsic inactivation/desensitization is expected to affect the shape of the olfactory response in vivo. It will accelerate the termination of the odor-induced receptor current, and is consistent with the observation that the receptor current declines more rapidly than the ciliary Ca^{2+} signal (Reisert and Matthews, 2001b).

Determination of Channel Density by the Ca-buffer Method

The distance between Ca-permeable channels and Ca-activated channels can be measured with biochemical or biophysical techniques (e.g., chemical cross-linking or FRET) if the channels are no more than ∼1–2 nm apart, or with immunofluorescence methods if the distance is within the resolution limit of light microscopy (∼1 μm). However, these methods require knowledge of the molecular identity of the proteins involved, which is absent for the olfactory Ca-activated Cl channel. Here we describe a method that fills the gap between these techniques and permits measurements of mean distances in the range of several hundred nanometers. Our quantitative analysis of channel densities is based on insights into buffered Ca^{2+} diffusion near Ca channels (Neher, 1986; Bauer, 2001). This approach is in principle applicable to any situation in which the effect of Ca buffers on Ca-dependent currents can be analyzed.

Application of the Ca-buffer method to the ciliary membrane of ORNs yielded several results: (a) evidence against the colocalization of CNG channels and Ca-activated Cl channels in transducisomes; (b) estimates for the densities of CNG channels and Cl channels and the distances between them; (c) an estimate for the lateral Ca^{2+}-diffusion coefficient on the cytoplasmic side of the ciliary membrane; (d) evidence that a number of CNG channels contribute to the local $[Ca^{2+}]_{free}$ sensed by each Cl channel; and (e) evidence for functional coupling, but against direct contact, between Cl channels and Na/Ca exchanger sites.

Functional Coupling between CNG and Cl Channels

Efficient functional coupling within a transduction cascade requires soluble messengers such as Ca^{2+} having to travel only short distances to reach their targets. In extreme cases, direct contact or organization into transducisome complexes between the transduction proteins can minimize the signal-transfer distance, as proposed for certain components of phototransduction in vertebrates (Korschen et al., 1999; Schwarzer et al., 2000; Poetsch et al., 2001; Bauer, 2002) and invertebrates (Zuker, 1996). Such an arrangement gives rise to a fast light response in *Drosophila* photoreceptors with

latencies as short as 2 ms (Tsunoda and Zuker, 1999). Here, we show that the transduction channels in ORNs are not constituents of transducisomes but are positioned ~120 nm apart. This finding indicates that olfactory signal transduction is not optimized for speed. On the other hand, ORNs are equipped with an unusual current amplification mechanism, in the form of a large Cl current triggered by a primary Ca current through CNG channels. In this respect, the olfactory CNG channels serve a somewhat different purpose from that of the CNG channels in vertebrate photoreceptors, which conduct the receptor current alone (for review see Kaupp and Seifert, 2002) and are expressed at ~30-fold higher density (300–500 μm^{-2} and 160 μm^{-2} in bovine and salamander rod outer segments; Bauer and Drechsler, 1992; Karpen et al., 1992). Interestingly, the number of CNG channels contributing significantly to the local Ca^{2+} concentration in the olfactory cilia appears to be much smaller than, for example, the number of voltage-activated Ca channels (~60) in the rat calyx of Held synapse necessary for the release of a single vesicle (Borst and Sakmann, 1996).

Although the Cl channel density on ORN ciliary membrane is comparable in both rat and frog, the CNG channel density is an order of magnitude lower in rat than previously found in frog (Larsson et al., 1997). This species difference may explain the considerably larger contribution of Cl current to the overall odor-induced current in mammals (>80%) than in amphibians (36–60%) (Kurahashi and Yau, 1993; Lowe and Gold, 1993; Zhainazarov and Ache, 1995). Kleene (1997) was the first to point out that, because of its small unitary current and high open probability, Ca-activated Cl channels can amplify the CNG current with little amplification of its current noise. The result is an increase in gain without an increase in noise. Our finding that each Cl channel monitors a rise in Ca^{2+} concentration contributed from multiple CNG channels means that some of the noise from individual CNG channels will be removed by spatial integration. In conclusion, the high Cl fraction of the rat olfactory receptor current is based on a roughly eightfold excess of Cl channels over CNG channels. The low-noise amplification results from smoothing of local [Ca^{2+}] fluctuations by summation of Ca profiles that originate from several CNG channels within a few hundred nm distance of each Cl channel.

J. Reisert is indebted to Dr. R.C. Thomas of the Physiological Laboratory, Cambridge, UK for assistance in determining the free Ca^{2+} concentrations in the solutions used.

This work was supported by the Deutsche Forschungsgemeinschaft (SPP 1025).

Olaf S. Andersen served as editor.

Submitted: 17 June 2003
Accepted: 22 July 2003

REFERENCES

Allbritton, N.L., T. Meyer, and L. Stryer. 1992. Range of messenger action of calcium ion and inositol 1,4,5-trisphosphate. *Science.* 258:1812–1815.

Balasubramanian, S., J.W. Lynch, and P.H. Barry. 1995. The permeation of organic cations through cAMP-gated channels in mammalian olfactory receptor neurons. *J. Membr. Biol.* 146:177–191.

Bauer, P.J. 2001. The local Ca concentration profile in the vicinity of a Ca channel. *Cell Biochem. Biophys.* 35:49–61.

Bauer, P.J. 2002. Binding of the retinal rod Na^+/Ca^{2+}-K^+ exchanger to the cGMP-gated channel indicates local Ca^{2+}-signaling in vertebrate photoreceptors. *Ann. NY Acad. Sci.* 976:325–334.

Bauer, P.J., and M. Drechsler. 1992. Association of cyclic GMP-gated channels and Na^+-Ca^{2+}-K^+ exchangers in bovine retinal rod outer segment plasma membranes. *J. Physiol.* 451:109–131.

Becq, F. 1996. Ionic channel rundown in excised membrane patches. *Biochim. Biophys. Acta.* 1286:53–63.

Blaustein, M.P., and W.J. Lederer. 1999. Sodium calcium exchange: Its physiological implications. *Physiol. Rev.* 79:763–854.

Borst, J.G., and B. Sakmann. 1996. Calcium influx and transmitter release in a fast CNS synapse. *Nature.* 383:431–434.

Bradley, J., D. Reuter, and S. Frings. 2001. Facilitation of calmodulin-mediated odor adaptation by cAMP-gated channel subunits. *Science.* 294:2176–2178.

Cervetto, L., L. Lagnado, R.J. Perry, D.W. Robinson, and P.A. McNaughton. 1989. Extrusion of calcium from rod outer segments is driven by both sodium and potassium gradients. *Nature.* 337: 740–743.

Chen, T.-Y., and K.-W. Yau. 1994. Direct modulation by Ca^{2+}-calmodulin of cyclic nucleotide-activated channel of rat olfactory receptor neurons. *Nature.* 368:545–548.

DeFelice, L.J. 1981. Introduction to Membrane Noise. Plenum Press, New York.

Dzeja, C., V. Hagen, U.B. Kaupp, and S. Frings. 1999. Ca^{2+} permeation in cyclic nucleotide-gated channels. *EMBO J.* 18:131–144.

Firestein, S., C. Picco, and A. Menini. 1993. The relation between stimulus and response in olfactory receptor cells of the tiger salamander. *J. Physiol.* 468:1–10.

Frings, S., J.W. Lynch, and B. Lindemann. 1992. Properties of cyclic nucleotide-gated channels mediating olfactory transduction. Activation, selectivity, and blockage. *J. Gen. Physiol.* 100:45–67.

Frings, S., D. Reuter, and S.J. Kleene. 2000. Neuronal Ca^{2+}-activated Cl^- channels—homing in on an elusive channel species. *Prog. Neurobiol.* 60:247–289.

Frings, S., R. Seifert, M. Godde, and U.B. Kaupp. 1995. Profoundly different calcium permeation and blockage determine the specific function of distinct cyclic nucleotide-gated channels. *Neuron.* 15:169–179.

Gold, G.H. 1999. Controversial issues in vertebrate olfactory transduction. *Annu. Rev. Physiol.* 61:857–871.

Goldstein, B.J., H.M. Kulaga, and R.R. Reed. 2003. Cloning and characterization of SLP3: a novel member of the stomatin family expressed by olfactory receptor neurons. *J. Assoc. Res. Otolaryngol.* 4:74–82.

Hallani, M., J.W. Lynch, and P.H. Barry. 1998. Characterization of calcium-activated chloride channels in patches excised from the dendritic knob of mammalian olfactory receptor neurons. *J. Membr. Biol.* 161:163–171.

Haynes, L.W., A.R. Kay, and K.-W. Yau. 1986. Single cyclic GMP-activated channel activity in excised patches of rod outer segment membrane. *Nature.* 321:66–70.

Hirakawa, Y., M. Gericke, R.A. Cohen, and V.M. Bolotina. 1999. Ca^{2+}-dependent Cl^- channels in mouse and rabbit aortic smooth muscle cells: regulation by intracellular Ca^{2+} and NO. *Am. J. Physiol.* 277:H1732–H1744.

Ismailov, I.I., C.M. Fuller, B.K. Berdiev, V.G. Shlyonsky, D.J. Benos, and K.E. Barrett. 1996. A biologic function for an "orphan" messenger: D-myo-inositol 3,4,5,6-tetrakisphosphate selectively blocks epithelial calcium-activated chloride channels. *Proc. Natl. Acad. Sci. USA.* 93:10505–10509.

Kaneko, H., T. Nakamura, and B. Lindemann. 2001. Noninvasive measurement of chloride concentration in rat olfactory receptor cells with use of a fluorescent dye. *Am. J. Physiol. Cell Physiol.* 280: C1387–C1393.

Karpen, J.W., D.A. Loney, and D.A. Baylor. 1992. Cyclic GMP-activated channels of salamander retinal rods: spatial distribution and variation of responsiveness. *J. Physiol.* 448:257–274.

Kaupp, U.B., and R. Seifert. 2002. Cyclic nucleotide-gated ion channels. *Physiol. Rev.* 82:769–824.

Kennedy, H.J., and R.C. Thomas. 1996. Effects of injecting calcium-buffer solution on $[Ca^{2+}]_i$ in voltage-clamped snail neurons. *Biophys. J.* 70:2120–2130.

Kleene, S.J. 1993. Origin of the chloride current in olfactory transduction. *Neuron.* 11:123–132.

Kleene, S.J. 1997. High-gain, low-noise amplification in olfactory transduction. *Biophys. J.* 73:1110–1117.

Kleene, S.J. 1999. Both external and internal calcium reduce the sensitivity of the olfactory cyclic-nucleotide-gated channel to cAMP. *J. Neurophysiol.* 81:2675–2682.

Kleene, S.J. 2000. Spontaneous gating of olfactory cyclic-nucleotide-gated channels. *J. Membr. Biol.* 178:49–54.

Kleene, S.J., and R.C. Gesteland. 1991. Calcium-activated chloride conductance in frog olfactory cilia. *J. Neurosci.* 11:3624–3629.

Korschen, H.G., M. Beyermann, F. Müller, M. Heck, M. Vantler, K.W. Koch, R. Kellner, U. Wolfrum, C. Bode, K.P. Hofmann, and U.B. Kaupp. 1999. Interaction of glutamic-acid-rich proteins with the cGMP signalling pathway in rod photoreceptors. *Nature.* 400: 761–766.

Kurahashi, T., and T. Shibuya. 1990. Ca^{2+}-dependent adaptive properties in the solitary olfactory receptor cell of the newt. *Brain Res.* 515:261–268.

Kurahashi, T., and K.-W. Yau. 1993. Co-existence of cationic and chloride components in odorant-induced current of vertebrate olfactory receptor cells. *Nature.* 363:71–74.

Larsson, H.P., S.J. Kleene, and H. Lecar. 1997. Noise analysis of ion channels in non-space-clamped cables: Estimates of channel parameters in olfactory cilia. *Biophys. J.* 72:1193–1203.

Leinders-Zufall, T., C.A. Greer, G.M. Shepherd, and F. Zufall. 1998. Imaging odor-induced calcium transients in single olfactory cilia: Specificity of activation and role in transduction. *J. Neurosci.* 18: 5630–5639.

Lindemann, B. 2001. Predicted profiles of ion concentrations in olfactory cilia in the steady state. *Biophys. J.* 80:1712–1721.

Lowe, G., and G.H. Gold. 1993. Nonlinear amplification by calcium-dependent chloride channels in olfactory receptor cells. *Nature.* 366:283–286.

Meinrenken, C.J., J.G. Borst, and B. Sakmann. 2003. Local routes revisited: the space and time dependence of the Ca^{2+} signal for phasic transmitter release at the rat calyx of Held. *J. Physiol.* 547:665–689.

Naraghi, M., and E. Neher. 1997. Linearized buffered Ca^{2+} diffusion in microdomains and its implications for calculation of $[Ca^{2+}]$ at the mouth of a calcium channel. *J. Neurosci.* 17:6961–6973.

Neher, E. 1986. Concentration profiles of intracellular calcium in the presence of a diffusible chelator. *In* Experimental Brain Research. Vol. 14. U. Heinemann, M. Klee, E. Neher, and W. Singer, editors. Springer, Heidelberg. 80–96.

Neher, E. 1998. Vesicle pools and Ca^{2+} microdomains: new tools for understanding their roles in neurotransmitter release. *Neuron.* 20:389–399.

Poetsch, A., L.L. Molday, and R.S. Molday. 2001. The cGMP-gated channel and related glutamic acid-rich proteins interact with peripherin-2 at the rim region of rod photoreceptor disc membranes. *J. Biol. Chem.* 276:48009–48016.

Reisert, J., and H.R. Matthews. 1998. Na^+-dependent Ca^{2+} extrusion governs response recovery in frog olfactory receptor cells. *J. Gen. Physiol.* 112:529–535.

Reisert, J., and H.R. Matthews. 2001a. Response properties of isolated mouse olfactory receptor cells. *J. Physiol.* 530:113–122.

Reisert, J., and H.R. Matthews. 2001b. Simultaneous recording of receptor current and intraciliary Ca^{2+} concentration in salamander olfactory receptor cells. *J. Physiol.* 535:637–645.

Reuter, D., K. Zierold, W.H. Schröder, and S. Frings. 1998. A depolarizing chloride current contributes to chemoelectrical transduction in olfactory sensory neurons in situ. *J. Neurosci.* 18:6623–6630.

Reuter, H., and N. Seitz. 1968. The dependence of calcium efflux from cardiac muscle on temperature and external ion composition. *J. Physiol.* 195:451–470.

Sato, K., and N. Suzuki. 2000. The contribution of a Ca^{2+}-activated Cl^- conductance to amino-acid-induced inward current responses of ciliated olfactory neurons of the rainbow trout. *J. Exp. Biol.* 203:253–262.

Schild, D., and D. Restrepo. 1998. Transduction mechanisms in vertebrate olfactory receptor cells. *Physiol. Rev.* 78:429–466.

Schlenker, T., and J.G. Fitz. 1996. Ca^{2+}-activated Cl^- channels in a human biliary cell line: regulation by Ca^{2+}/calmodulin-dependent protein kinase. *Am. J. Physiol.* 271:G304–G310.

Schreiber, S., J. Fleischer, H. Breer, and I. Boekhoff. 2000. A possible role for caveolin as a signaling organizer in olfactory sensory membranes. *J. Biol. Chem.* 275:24115–24123.

Schwarzer, A., H. Schauf, and P.J. Bauer. 2000. Binding of the cGMP-gated channel to the Na/Ca-K exchanger in rod photoreceptors. *J. Biol. Chem.* 275:13448–13454.

Sheng, M., and C. Sala. 2001. PDZ domains and the organization of supramolecular complexes. *Annu. Rev. Neurosci.* 24:1–29.

Thomas, M.V. 1982. Techniques in calcium research. Academic Press, London.

Tsunoda, S., and C.S. Zuker. 1999. The organization of INAD-signaling complexes by a multivalent PDZ domain protein in Drosophila photoreceptor cells ensures sensitivity and speed of signaling. *Cell Calcium.* 26:165–171.

Wang, Y.X., and M.I. Kotlikoff. 1997. Inactivation of calcium-activated chloride channels in smooth muscle by calcium/calmodulin-dependent protein kinase. *Proc. Natl. Acad. Sci. USA.* 94: 14918–14923.

Xie, W., K.R. Solomons, S. Freeman, M.A. Kaetzel, K.S. Bruzik, D.J. Nelson, and S.B. Shears. 1998. Regulation of Ca^{2+}-dependent Cl^- conductance in a human colonic epithelial cell line (T84): cross-talk between Ins(3,4,5,6)P4 and protein phosphatases. *J. Physiol.* 510:661–673.

Zhainazarov, A.B., and B.W. Ache. 1995. Odor-induced currents in Xenopus olfactory receptor cells measured with perforated-patch recording. *J. Neurophysiol.* 74:479–483.

Zimmerman, A.L., J.W. Karpen, and D.A. Baylor. 1988. Hindered diffusion in excised membrane patches from retinal rod outer segments. *Biophys. J.* 54:351–355.

Zufall, F., and S. Firestein. 1993. Divalent cations block the cyclic nucleotide-gated channel of olfactory receptor neurons. *J. Neurophysiol.* 69:1758–1768.

Zufall, F., T. Leinders-Zufall, and C.A. Greer. 2000. Amplification of odor-induced Ca^{2+} transients by store-operated Ca^{2+} release and its role in olfactory signal transduction. *J. Neurophysiol.* 83:501–512.

Zuker, C.S. 1996. The biology of vision of *Drosophila. Proc. Natl. Acad. Sci. USA.* 93:571–576.